hess-2022-121 – Author's response to Anonymous Referee 1

Matthias Forkel[1], Luisa Schmidt[1], Ruxandra-Maria Zotta[2], Wouter Dorigo[2], and Marta Yebra[3,4]

[1] Technische Universität Dresden, Institute of Photogrammetry and Remote Sensing, 01062 Dresden, Germany
[2] Technische Universität Wien, Department of Geodesy and Geoinformation, 1040 Vienna, Austria
[3] Fenner School of Environment and Society, Australian National University, ACT 2601, Australia
[4] School of Engineering, Australian National University, ACT 2601, Australia

Correspondence to: Matthias Forkel (matthias.forkel@tu-dresden.de)

Referee comments are written in blue italics; author's responses are written in normal font; and proposed changes are highlighted in green font.

The manuscript "Estimating leaf moisture content at global scale from passive microwave satellite observations of vegetation optical depth" presents developing a global scale LFMC estimation model using vegetation optical depth from passive microwave satellite data. Although LFMC is well known to be a critical component on estimating wildfire potential, little studies have been done on global studies yet. The large target region makes this study unique compared to the previous studies focusing on regional or local scale. Authors reasonably well deliver the new LFMC model development process. However, there are a couple of major concerns described below.

We thank the referee for the time and effort to provide a critical review that will help to improve the manuscript. We hope that we addressed all comments appropriately.

Major comments

Section 2.6: authors employed 4 models (Model A to D). Where those models come from? Do authors created those equations or from previous studies? If so, it needed to be specified the references of each model.

We understand that our text is not clear enough about how we derived those models. We developed those models either based on regressions by assuming positive relations between LFMC and VOD (models A and B) or by adopting existing model approaches that link VOD with biomass, VWC and LFMC (models C and D). We propose to change the text in section 2.6 as follows to make the origin of the models clear:

We developed tested four different models to estimate daily LFMC from daily values of VOD. All models were developed in this study either by assuming non-linear regressions between LFMC and VOD or by adopting known relations between LFMC, VOD, VWC and dry biomass from previous studies (Jackson and Schmugge, 1991; Sawada et al., 2016; Frappart et al., 2020). Specifically, in models A and B we assume a positive relationship between VOD and LFMC and use logistic regression (S-shaped curve) to estimate LFMC from VOD. We use logistic regression because LFMC cannot be smaller than 0% and LFMC

values higher than 200% are rare (the 95-percentile of LFMC is 193%, the maximum is 549% in the Globe-LFMC database). In models C and D, we adopt the relationships between LFMC, VWC and dry biomass (equation 1) and between VOD and VWC (equation 2) to calculate LFMC. The four models are described with more detail in the following paragraphs. Each model has up to four model parameters. Prior ranges and values of those model parameters were manually selected in order to always obtain a positive relationship between VOD and LFMC and to obtain typical LFMC values (Table 2).

In **Model A**, we assume that LFMC is directly proportional to VOD by using a logistic regression:

$$LFMC = \frac{LFMC_{max}}{1+e^{-sl\times(VOD-VOD_0)}} \quad (4)$$

Where $LFMC_{max}$ is the maximum possible LFMC value (in %) and sl is the slope of the curve. VOD_0 is the inflection point of the logistic curve, i.e. the VOD value at which half of the LFMC between 0% and $LFMC_{max}$ is reached. The parameters $LFMC_{max,}$ sl and VOD_0 were calibrated for each site.

In **Model B**, we additionally assume that LFMC depends on seasonal changes in canopy structure. Therefore, we additionally include monthly-averaged LAI as predictor. We assume that LFMC can be expressed based on a weighted combination x of daily VOD and monthly-averaged LAI. Like in model A, we use a logistic regression in order to limit LFMC between 0% and $LFMC_{max}$:

$$x = f \times VOD + (1-f) \times LAI \quad (5)$$

$$LFMC = \frac{LFMC_{max}}{1+e^{-sl\times(x-x_0)}} \quad (6)$$

Where f is a fraction between zero and one that regulates if VOD (f = 1) or LAI (f = 0) contributes more to the calculation of x and hence to LFMC. sl and $x0$ are the slope and inflection point of the logistic curve. Note that we kept the parameter $LFMC_{max}$ constant at 400% in model B (corresponding to the 99.99%-ile of LFMC in the Globe-LFMC database) throughout all analyses because the calibration results from model A have shown that any high value for $LFMC_{max}$ is not sensitive for the performance of the estimated LFMC.

For **Model C** we directly made use of the VOD-LFMC relationship presented in equation 2 (Jackson and Schmugge, 1991; Konings et al., 2019) and compute LFMC by solving this equation for LFMC:

$$LFMC = \frac{VOD}{b \times m_{dry}} \times 100\% \quad (7)$$

To account for dry biomass of the canopy, we assume a linear relation with monthly-averaged LAI:

$$m_{dry} = a \times LAI + c \quad (8)$$

For the parameter b in equation 7, a prior value of 1.5 with a range between 0.1 and 4 was taken based on the values presented in Jackson and Schmugge (1991). The parameter a was varied between 0.01 and 100 as dry canopy biomass should positively scale with LAI. The parameter c is the intercept of this linear regression and was chosen around zero (between -10 and 10). Note that the parameters a and b are directly positively correlated in model C and could indeed be represented by a combined product. However, as we have both prior information on the values of b (i.e. VOD-VWC relation) and a (i.e. the relation between leaf mass and leaf area) but not on their combined product, we decided to keep the two factors separated.

We developed **Model D** by using the basic definition of FMC (equation 1) and compute LFMC as the ratio between VWC and dry biomass:

$$LFMC = \frac{VWC}{m_{dry}} \times 100\% \quad (9)$$

Thereby, we compute VWC based on a exponential relationship between LAI and VWC (Paloscia and Pampaloni, 1988; Sawada et al., 2016) and compute dry biomass by assuming a positive relationship between VOD and biomass (e.g. Frappart et al., 2020). Following Sawada et al. (2016), VWC is computed based on an exponential relationship with LAI:

$$VWC = e^{\frac{LAI}{k}} - 1 \quad (10)$$

Where the parameter *k* defines the shape of the exponential relationship. As we have no prior information about the value of *k*, we sampled *k* over a large range (0.1 - 100). The computation of dry biomass is based on a linear relation with VOD which is based on the assumption that VOD at short wavelengths is proportional to canopy biomass (Frappart et al., 2020):

$$m_{dry} = a \times VOD + c \quad (11)$$

The parameters *a* and *c* define like in model C the relation with dry biomass.

Authors used random forest model to find out parameter of Model B. Have you tried RF model for the global LFMC model? It looks like utilizing RF model directly for the LFMC estimation is more reasonable and may show better model performance.

Originally, we did not consider a global random forest (RF) model to predict LFMC directly because we wanted to investigate the type of relationship between VOD and LFMC and their dependence on land cover by using the formulations in models A-D, which are based on previous studies (especially models C and D). Inferring such relationships from a fitted RF model is more complicated because it would require the use of methods from explainable machine learning such as for example partial dependencies or Shapley Additive Explanations.

However, as we are curious to test how a global RF performs in comparison to models A-D, we now trained a global RF model by using the same set of predictors that we also used for model B (i.e. daily Ku-VOD, monthly LAI, and tree cover). The global training of the RF was performed with the same spatial cross-validation procedure like for the other models, i.e. with the same set of 20 folds of spatially-clustered LFMC sites. We used 100 decision trees in the RF of each sample.

The results of the spatial cross-validation for the RF are compared against the other models in Figure AC1 1. The RF achieved correlations of $0.50^{0.77}_{0.18}$ and RMSE of $40^{79.5}_{21.9}$%-LFMC in spatial cross-validation between observed and estimated LFMC. While this performance is comparable to the other models, the RF performed in average slightly better than the best-performing model B in terms of RMSE (median RMSE: 40% RF, 48.8% model B) but worse than model B and D in terms of correlation (median correlation: 0.50 RF, 0.58 model B).

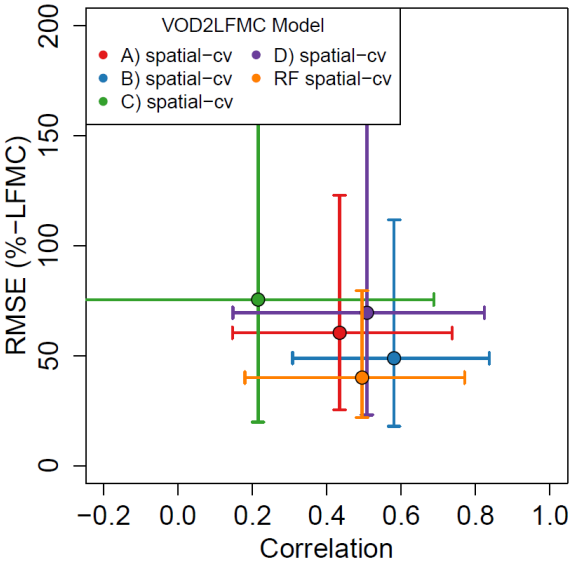

Figure AC1 1: Performance of the global random forest (RF, orange) in comparison with models A-D using Ku-VOD after using sites as test data in spatial cross validation. Shown is the root mean squared error (RMSE) and correlation coefficient between estimated and measured LFMC. Dots and bars are the median and range from the 5 to 95%-iles across all sites, respectively.

We also investigated the performance of the RF model for different sites and vegetation growth forms in terms of the Kling-Gupta efficiency (KGE) like we did this for model B in the main text (Figure AC1 2 and Figure 7 of the main text). The differences in model performance of RF between vegetation types are comparable to the results that we found for model B. While RF achieved lesser very low KGE values than model B, model B had in average higher KGE values. We found the highest performance of RF for shrubs (median KGE = 0.3 for RF and 0.4 for model B) and forbs (0.28 for RF and 0.32 for model B), lower performance for broad-leaved trees (0.18 for RF and 0.25 for model B) and low performance for needle-leaved trees (-0.14 for RF and -0.49 for model B).

Those results are indeed insightful because they confirm on the one hand the value and robustness of the best-performing model B, which can better reproduce the temporal dynamic of observed LFMC (as indicated by the higher correlation) than the RF model. On the other hand, it shows the potential of RF to further improve the estimation of LFMC because further predictor variables can be potentially included.

Despite the value of those results, we propose to not include them in the revised manuscript because they would add more complexity to the already complex analysis and would complicate the logic order of the text. However, we could discuss the possibility of using RF directly in the discussion and refer to the analysis in this Author's Response.

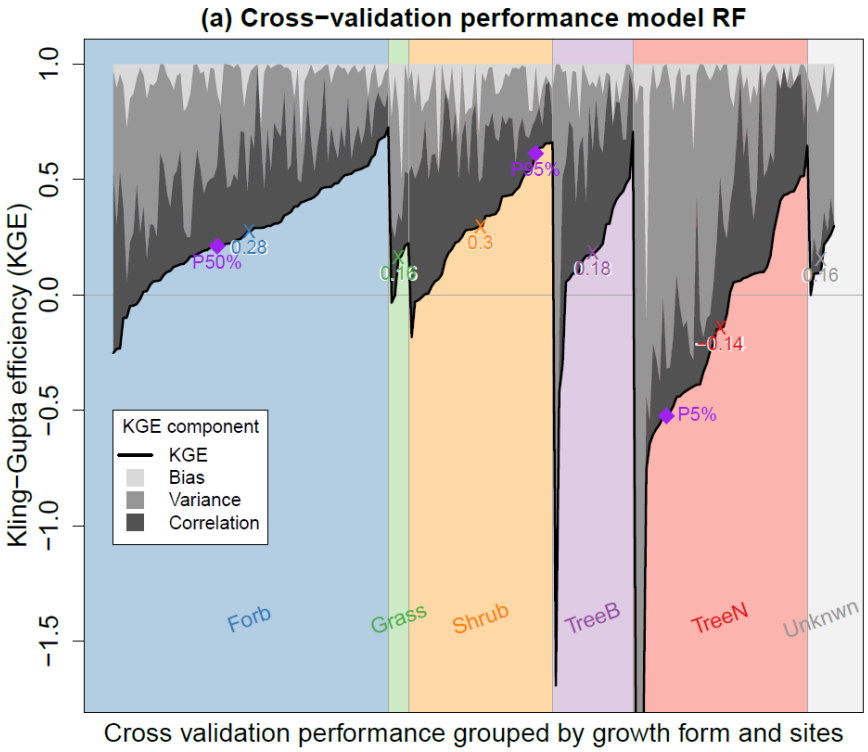

Figure AC1 2: Performance of the RF model in spatial cross validation at each site grouped by the sampled vegetation growth form of LFMC measurements. Figure 7 of the main text provides the same type of analysis for model B and provides further explanations.

Section 3.3.1: Model performance looks fine overall. However, the needle-leaved tree has specifically poor performance. This is not because of your model calibration issue but non-linear relationship between soil moisture and vegetation moisture of needle-leaved trees. Do you think it is necessary to include this type of vegetation on LFMC model based on VOD?

We do not fully understand this question of the referee but try to provide an explanation. Soil moisture is not included on our models because we assume that any temporal dynamics in LFMC can be estimated from temporal changes in daily VOD and monthly LAI as those variables represent changes in vegetation water content and canopy biomass. This assumption is valid also for needle-leaved trees because we achieved good performances in estimating LFMC in site-level calibration (e.g. median RMSE = 15% for needle-leaved trees, Figure 5).

However, the performance for needle-leaved trees is much lower in spatial cross-validation, which indicates that the calibrated parameters from each site cannot be well estimated in space. We assume that this is caused by the spatial representativeness of the used LFMC sites with needle-leaved trees within spatial cross-validation. All of the used sites with needle-leaved trees are located in the western US and most of the sites are located in regions with low tree cover (Figure AC1 3). Only a few sites are located in regions with higher tree cover and those sites are distributed across different spatial clusters for cross-validation.

Needle-leaved trees are included in 11 out of 20 spatial clusters and six of the spatial clusters include less than three sites with needle-leaved trees. This implies that in such cases the training of model parameters is mostly based on sites with other vegetation types and from other regions, which will likely result in a low performance for needle-leaved trees.

We propose to include this explanation in the discussion of the results in section 3.2.2.

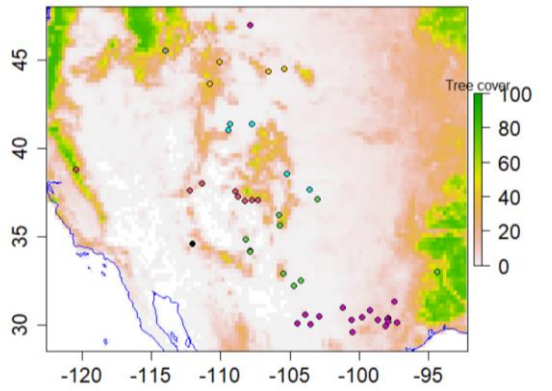

Figure AC1 3: Location of the Globe-LFMC sites with needle-leaved trees that were used for model calibration. Colours denote sites that were included in the same spatial cluster for spatial cross-validation.

Section 3.4: One of the important roles of the coarse resolution with global scale model is to show the large-scale spatiotemporal patterns. However, global LFMC model validation using seasonal variation at single year is not enough. (e.g. Fig.8) It need to be shown that model can represent the continent levels interannual anomalies such as multi-year drought cases in the western US, Australia or other regions.

This is a very good suggestion. We performed an analysis of drought conditions in North America and specifically in California by comparing the VOD-based LFMC estimates from model B with the 12-monthly Standardized Precipitation Index (SPI-12) and the U.S. Drought Severity and Coverage Index (DSCI) (Figure AC1 4). SPI-12 data was taken from the Global Drought Observatory (Global Drought Observatory - JRC European Commission, 2022) and DSCI data from the U.S. Drought Monitor (U.S. Drought Monitor, 2022). August 2014 was one of the most severe drought months in the western U.S. The VOD-based LFMC estimates show wide-spread patterns of very low LFMC over the western U.S. during this month (Figure AC1 4 a). This corresponds to a lack in precipitation as indicated by the negative SPI-12 (Figure AC1 4 b). Also large regions in northern Canada show precipitation deficit with low SPI-12 in northern Canada, which also corresponds to patterns of low LFMC. To investigate multi-year drought cases, we also compared LFMC, SPI-12 and DSCI time series averaged for the state of California as an example (Figure AC1 4 c). Both SPI-12 and the DSCI show the multi-year drought between 2013 and 2016. The LFMC time series is dominated by the strong seasonal signal. Therefore, we decomposed the LFMC time series for California into a seasonal, trend and remainder component using the STL (seasonal decomposition of time series by Loess)

method. The LFMC trend shows a long period of low values between 2013 and 2016, which corresponds to the drought period. Also the wet period between 2005 and 2007 with higher precipitation (i.e. high SPI-12) and no drought conditions (i.e. DSCI close to 0) corresponds to high LFMC values. The LFMC trend component is medium correlated with SPI-12 (r = 0.495) and DSCI (r = -0.515) and hence reflects well the inter-annual variability of drought and wet conditions. This continental/regional case study demonstrates the potential to investigate multi-year drought conditions with the VOD-based LFMC estimates.

We propose to include this analysis in the revised version of the manuscript, which demonstrates that the model can represent multi-year drought cases. However, we think a further comparison with drought conditions in other regions is beyond the scope of the manuscript and will further increase the length of the manuscript.

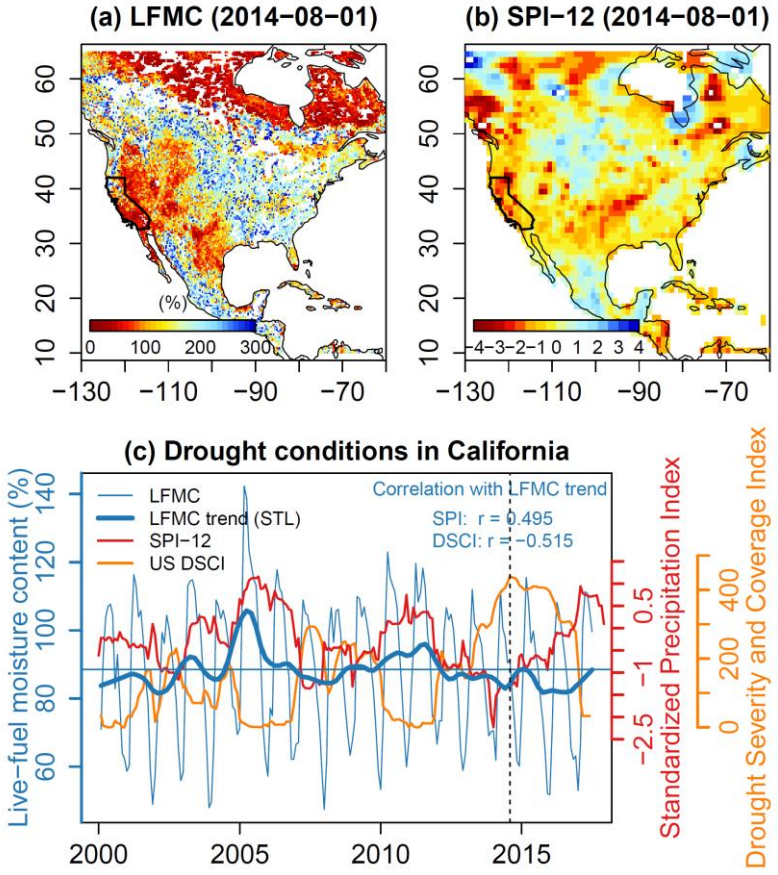

Figure AC1 4: Comparison of LFMC as derived from model B with drought conditions in North America and California. (a) Map of mean monthly LFMC for August 2014, a month with severe drought in the western United States. The state of California is highlighted in the map. (b) Map of the Standardized Precipitation Index for 12-monthly accumulation periods (SPI-12) for August 2014. SPI-12 data is taken from GDO (2021). (c) Comparison of LFMC, SPI-12 and the US Drought Severity and Coverage Index (DSCI) for California. DSCI data is taken from the U.S. Drought Monitor (2022). To analyse inter-annual variability in LFMC, we computed the trend in LFMC based on the STL time series decomposition method (seasonal decomposition of time series by Loess). A severe drought started in California (and in the western US) in 2013 and lasted until end 2016 as shown by negative SPI-12 values, very high DSCI values, and low LFMC.

Minor comments

Figure 3 x-axis label is confusing. Change [0,20] to 0~20%

We will change this.

Line 710 "procuts"

We will change this.

References

Global Drought Observatory - JRC European Commission: https://edo.jrc.ec.europa.eu/gdo/php/index.php?id=2112, last access: 18 July 2022.

Frappart, F., Wigneron, J.-P., Li, X., Liu, X., Al-Yaari, A., Fan, L., Wang, M., Moisy, C., Le Masson, E., Aoulad Lafkih, Z., Vallé, C., Ygorra, B., and Baghdadi, N.: Global Monitoring of the Vegetation Dynamics from the Vegetation Optical Depth (VOD): A Review, Remote Sens., 12, 2915, https://doi.org/10.3390/rs12182915, 2020.

Jackson, T. J. and Schmugge, T. J.: Vegetation effects on the microwave emission of soils, Remote Sens. Environ., 36, 203–212, https://doi.org/10.1016/0034-4257(91)90057-D, 1991.

Konings, A. G., Rao, K., and Steele-Dunne, S. C.: Macro to micro: microwave remote sensing of plant water content for physiology and ecology, New Phytol., 223, 1166–1172, https://doi.org/10.1111/nph.15808, 2019.

Paloscia, S. and Pampaloni, P.: Microwave polarization index for monitoring vegetation growth, IEEE Trans. Geosci. Remote Sens., 26, 617–621, https://doi.org/10.1109/36.7687, 1988.

Sawada, Y., Tsutsui, H., Koike, T., Rasmy, M., Seto, R., and Fujii, H.: A Field Verification of an Algorithm for Retrieving Vegetation Water Content From Passive Microwave Observations, IEEE Trans. Geosci. Remote Sens., 54, 2082–2095, https://doi.org/10.1109/TGRS.2015.2495365, 2016.

U.S. Drought Monitor: https://droughtmonitor.unl.edu/DmData/DataDownload/DSCI.aspx, last access: 18 July 2022.